Environmental Science & Technology

pubs.acs.org/est

Article

Enzymes, Manganese, or Iron? Drivers of Oxidative Organic Matter Decomposition in Soils

Morris E. Jones, Rachelle E. LaCroix, Jacob Zeigler, Samantha C. Ying, Peter S. Nico, and Marco Keiluweit*

Cite This: *Environ. Sci. Technol.* 2020, 54, 14114–14123

Read Online

ACCESS | Metrics & More | Article Recommendations | Supporting Information

ABSTRACT: Oxidative decomposition of soil organic matter determines the proportion of carbon that is either stored or emitted to the atmosphere as CO_2. Full conversion of organic matter to CO_2 requires oxidative mechanisms that depolymerize complex molecules into smaller, soluble monomers that can be respired by microbes. Current models attribute oxidative depolymerization largely to the activity of extracellular enzymes. Here we show that reactive manganese (Mn) and iron (Fe) intermediates, rather than other measured soil characteristics, best predict oxidative activity in temperate forest soils. Combining bioassays, spectroscopy, and wet-chemical analysis, we found that oxidative activity in surface litters was most significantly correlated to the abundance of reactive Mn(III) species. In contrast, oxidative activity in underlying mineral soils was most significantly correlated to the abundance of reactive Fe(II/III) species. Positive controls showed that both Mn(III) and Fe(II/III) species are equally potent in generating oxidative activity, but imply conventional bioassays have a systematic bias toward Fe. Combined, our results highlight the coupled biotic-abiotic nature of oxidative mechanisms, with Mn-mediated oxidation dominating within Mn-rich organic soils and Fe-mediated oxidation dominating Fe-rich mineral soils. These findings suggest microbes rely on different oxidative strategies depending on the relative availability of Fe and Mn in a given soil environment.

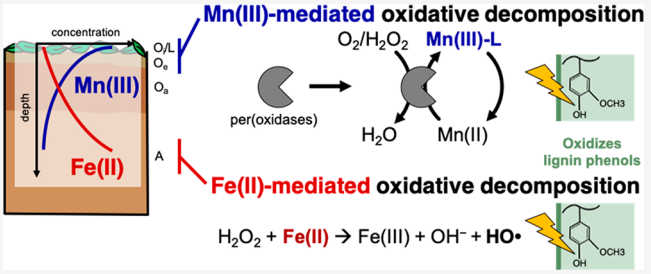

INTRODUCTION

Soils are one of the largest and most dynamic carbon (C) reservoirs on earth, storing more than three times as much C as the atmosphere and biosphere combined in the form of organic matter.[1] Oxidative decomposition of organic matter dictates the proportion of C in soils that is either stored or emitted into the atmosphere as CO_2 efflux;[2] even small changes in decomposition rate may thus cause adverse feedbacks to the climate system. Future predictions of soil carbon-climate feedbacks thus rely on accurate understanding of the mechanisms controlling decomposition and how they may respond to climate change.[3]

In decomposition, oxidative depolymerization of larger macromolecules such as lignin into smaller soluble compounds that can be assimilated and respired by microbes is often the rate limiting step.[4] This process is thought to require oxygen as well as extracellular enzymes that catalyze the oxidation reaction.[5] Soil C cycling models used to predict climate change impacts therefore increasingly incorporate measures of extracellular enzyme production and activity.[6,7] However, it is increasingly clear that purely enzymatic reactions alone do not explain the oxidative activity observed in soils, prompting questions about the representation of oxidative decomposition in models.[8] A number of recent studies suggest that a significant amount of oxidative decomposition and CO_2 production is due to nonenzymatic or abiotic reactions.[9−11] A possible explanation is the presence of reactive metal intermediates such as Mn and Fe species, which mediate the oxidation of macromolecules by molecular oxygen, and have been shown to enhance oxidative decomposition in soil systems as diverse as croplands,[12] forests,[13,14] peatlands,[15] and wetlands.[16,17]

Across the tree of life, soil microbes and fungi in particular employ several depolymerization strategies that utilize reactive Mn or Fe intermediates in coupled biotic-abiotic reactions.[18] Microbes can produce extracellular enzymes that oxidize Mn(II) to form soluble and reactive Mn(III) intermediates.[19] Basidiomycete fungi such as "white rots", for instance, produce oxidases, peroxidases, or ligninases that are implicated in the production of soluble Mn(III)-ligand complexes,[19,20] which are assumed to be potent oxidants of aromatic and phenolic structures. Moreover, several fungal and bacterial groups are known to oxidize Mn(II) nonenzymatically.[21] In contrast,

Received: June 27, 2020
Revised: October 8, 2020
Accepted: October 8, 2020
Published: October 23, 2020

https://dx.doi.org/10.1021/acs.est.0c04212
Environ. Sci. Technol. 2020, 54, 14114−14123

fungal groups such as saprotrophic "brown rots" or ectomycorrhiza, employ nonenzymatic depolymerization strategies that utilize Fe(II).[22−24] These organisms reduce Fe(III) to Fe(II) and release hydrogen peroxide (H_2O_2) to stimulate Fenton chemical reactions,[18] which produce soluble reactive oxygen species (e.g., hydroxyl radicals or superoxide) to nonspecifically oxidize macromolecules.[25] It is important to note that reactive oxygen species are not only produced biotically as described above but also abiotically in redox-active soils.[13,26] Abiotic Fe(II) oxidation by O_2 can produce H_2O_2, with subsequent Fenton reactions between H_2O_2 and Fe(II) producing reactive oxygen species.[13,27] Both Mn- and Fe-mediated depolymerization strategies thus produce soluble oxidants that are sufficiently small and potent to penetrate, oxidize, and depolymerize intact macromolecular structures.

Here we aimed to quantify the relative contribution of Mn- and Fe-mediated oxidative decomposition in forest soils. In most soils, Fe is more than 10 times as abundant as Mn.[1] However, plant uptake concentrates Mn in foliar tissue and subsequently accumulates Mn in forest floor litter layers.[28,29] Consequently, Mn concentrations often show a maximum in organic surface layers, where they are equal to or even exceed Fe concentrations.[30] We thus hypothesized that Mn-mediated oxidative decomposition would dominate in litter layers, while Fe-mediated mechanisms would control oxidative decomposition in the underlying mineral horizons. To test this hypothesis, we linked oxidative activity to variations in metal speciation and other soil characteristics in temperate deciduous forest soils. We chose depth profiles along a lowland-to-upland transect that exhibit strong moisture-induced gradients in redox conditions and, hence, variations in Mn and Fe abundance and speciation. We characterized reactive Mn and Fe phases along the transect using selective extractions and X-ray absorption near-edge fine structure (XANES) spectroscopy. To assess potential for oxidative decomposition, we used L-3,4-dihydroxyphenylalanine (L-DOPA), a hydroxy-aromatic probe widely used in colorimetric assays to assess oxidative activity in soils.[5,31,32] L-DOPA assays are traditionally conducted with and without the addition of H_2O_2, which is meant to distinguish the activity of H_2O_2-independent "oxidases" from the activity of H_2O_2-dependent "peroxidases". Because H_2O_2 is known to inhibit Mn(III) formation[33] and to enhance Fe(II)-mediated Fenton reactions,[34] we further examined potential biases of the L-DOPA assay toward either Mn- or Fe-mediated oxidation in soils amended with reactive metal phases. The utility of the L-DOPA probe in assessing both abiotic and biotic contributions to oxidative activity in soils are discussed.

METHODS

Soil Sampling. Samples were collected at the Harvard Forest Long-term Ecological Research site near Petersham, Massachusetts (42.54° N, 72.18° W). Samples were collected along a well-characterized upland-to-wetland transition surrounding a seasonal wetland complex[35] characteristic of ephemeral wetlands in the Northeastern U.S.,[36] which exhibit seasonal and temporal variations in redox conditions that manifest themselves in variations in metal speciation.[37] Soils are sandy loams classified as Typic Dystrudepts of the Gloucester series. The secondary forest is dominated by red oak (*Quercus rubra*), paper birch (*Betula papyrifera M.*), red and striped maple (*Acer rubrum L., Acer pennsylvanicum L.*), and white ash (*Fraxinus mericana L.*), which supply the majority of the leaf litter. Three positions termed "dry", "transition", and "wet", each separated by 3−5 m, were sampled along the established upland-to-wetland transect. At each position, we collected four replicate soil cores using a push-corer. In each core, we separated the partially decomposed litter layer (fresh leaf litter and O_i horizon, thickness = 4−6 cm) from the underlying organic (O_e and O_a, 7−9 cm) and the mineral (A_h, 15−20 cm) horizons, which were immediately stored anaerobically in mason jars with a small amount of dry ice to prevent changes in redox conditions. Jars were capped with an airtight lid with a septum to release CO_2 gas once sealed. Samples were transported on ice and transferred to an anaerobic chamber on the same day. In the chamber, coarse roots and twigs were removed before samples were gently ground and sieved to <590 μm.

Oxidative Activity Assays. Potential oxidative activity in each sample was assessed using the oxidation of the simple hydroxy-aromatic L-DOPA molecule. L-DOPA oxidation was examined in soil slurries with and without addition of H_2O_2, including appropriate controls, as described in Bach et al.[31] and recorded using a microplate spectrophotometer (Epoch 3, Biotek Instruments, Winooski, VT). To complete the assays, approximately 1 g of fresh soil was suspended in 125 mL of 50 mM pH 4.7 sodium acetate buffer to form a slurry in a blender (Lab 2 Speed 1L, Waring, Stamford, CT) at 18,000 rpm for 1 min. Assays were conducted with a 1:1 ratio of soil slurry and 25 mM L-DOPA substrate (with or without 0.3% H_2O_2) in 96-well plates. Because of the presence of heterogeneous soil debris in plates, we transferred 50 μL aliquots of a spun-down 100 μL aliquot of the assay solution to a new plate for spectrophotometric measurements.[38] For soil assays, we calculated oxidative activity based on the 4 h reading at 460 nm, as this is the time frame over which activity increased most linearly. Sixteen replicate wells were assayed for each sample. An extinction coefficient of 7.9/μmol was assumed.[32] Oxidative activity was calculated relative to controls without L-DOPA. In the following, we refer to assays without H_2O_2 as "baseline oxidative activity" (or "$-H_2O_2$"), the difference between assays with and without H_2O_2 addition as the potential "H_2O_2-dependent oxidative activity" (or "$+H_2O_2$"), and oxidative activity in assays with H_2O_2 additions as potential "total oxidative activity". Positive controls, in which we added reactive Mn and Fe species, were performed on the litter sample with the lowest overall activity. Assays were performed as described above and read after approximately 0.3, 1, 4, 16, and 24 h, but each well received either Mn(II)Cl_2, Mn(III)-pyrophosphate,[39] Fe(II)Cl_2, or Fe(III)Cl_3 to achieve concentrations of 1, 3, 12, or 38 μM upon initiation of the reaction. These treatments were chosen to mimic dissolved Mn(II), Mn(III)-ligand complexes, Fe(II), and Fe(III) phases. The concentration range (approximately 7−266 μg Fe or Mn g^{-1} soil) was chosen to cover the range of extractable Mn and Fe concentrations in our litter layer (Figure S-1). All standards were prepared in the anaerobic glovebag and assays were conducted under aerobic conditions in the dark.

Characterization of Reactive Mn and Fe Phases. Reactive Mn and Fe phases were characterized using soils dried in the anaerobic glovebag. Organically complexed Mn was targeted with a pyrophosphate extraction.[40,41] While the extraction targets both Mn(II) and Mn(III), ligands such as pyrophosphate will have much greater affinity for Mn(III).[42] Briefly, 0.5 g of soil was extracted with 10 mL of 0.1 M Na-pyrophosphate (at pH 10) with shaking for 1 h followed by

https://dx.doi.org/10.1021/acs.est.0c04212
Environ. Sci. Technol. 2020, 54, 14114−14123

Table 1. Basic Soil Characteristics of Surface Litter (L) As Well As Organic (O) and Mineral (A) Soils Across the Wetland-Upland Transect[a]

position	horizon	total C	C/N	microbial biomass C	water-extractable C	pH	total Mn[b]	total Fe[b]
		%	ratio	mg g^{-1}	mg g^{-1}		μg g^{-1}	mg g^{-1}
dry	L	49(2)	44	5.3(0.4)	1.06(0.09)	4.6(0.1)	306(9)	0.5(0.3)
	O	32(3)	30	2.7(0.3)	0.31(0.05)	3.7(0.2)	120(14)	10(1)
	A	1.8(0.4)	27	1.7(0.2)	0.07(0.01)	4.1(0.1)	244(12)	36(2)
transition	L	48(1)	31	4.0(0.4)	0.85(0.13)	4.3(0.1)	281(28)	0.4(0.1)
	O	32(6)	24	4.7(0.6)	0.48(0.23)	3.7(0.2)	123(26)	7(3)
	A	7(3)	17	2.1(0.4)	0.07(0.01)	4.8(0.1)	227(15)	13(3)
wet	L	45(2)	27	3.5(0.3)	0.81(0.16)	5.7(0.1)	223(8)	1.1(0.1)
	O	37(7)	27	2.6(0.2)	0.13(0.02)	5.0(0.2)	62(11)	4(2)
	A	9(4)	24	1.1(0.2)	0.05(0.01)	4.2(0.1)	244(27)	7(1)

[a]Parentheses indicate standard error of the mean (n = 4). [b]Determined by X-ray fluorescence (XRF).

centrifugation and filtration through 0.2-μm syringe filters. To determine the abundance of Fe(II) and Fe(III), 0.33 g of dried sample was extracted in 10 mL of 0.5 M HCl for 4 h, centrifuged (1 h at 4000 RCF), and filtered (0.22-μm). Concentrations of Fe(II) and Fe(III) in the supernatant were quantified in the dark using the ferrozine assay.[43] Changes in the solubility and reducibility of dominant Mn and Fe phases across the transect were assessed by a sequential extraction. Extraction by ultrapure H_2O ("water-soluble pool") was followed by ammonium acetate ("exchangeable pool"[44]), acidified hydroxylamine ("easily reducible pool"[45]), and dithionite-HCl ("total reducible pool"[44]). Briefly, 0.33 g of dried sample was added to 15 mL centrifuge tubes with 10 mL of ultrapure H_2O (18.3 M-ohm cm). Extracts were shaken for 1 h at 120 rpm, followed by centrifugation (1 h at 4000 RCF) and filtration of the supernatant through 0.22-μm syringe filters. The remaining soil pellet was resuspended in 10 mL of 1M ammonium acetate (pH = 7), shaken for 4 h (120 rpm), and centrifuged (1 h at 4000 RCF). Then 10 mL of 0.25 M hydroxylamine hydrochloride in 0.25 M hydrochloric acid, shaken for 4 h (120 rpm), and centrifuged (1 h at 4000 RCF). Residues were rinsed with 10 mL of deionized water, and combined extracts were filtered. The remaining soil pellet was resuspended in 10 mL of 0.05 M sodium dithionate, shaken for 16 h (120 rpm), centrifuged (1 h at 4000 RCF), and filtered. The residues were washed with 0.05 M HCl for 1 h, centrifuged, filtered, and combined with the dithionite extract. All extracts were acidified with 3% HNO_3 and analyzed for Mn and Fe by ICP-MS (Shimadzu ICPMS-2030).

To further speciate Mn, solid samples were analyzed by Mn K-edge X-ray absorption near-edge fine structure (XANES) spectroscopy at the wiggler beamline 4−3 at the Stanford Synchrotron Radiation Lightsource. Replicate samples were homogenized and combined into one composite sample (at equal mass ratio) and mounted in sample holders, sealed with X-ray transparent Kapton tape, and stored anaerobically prior to analysis. Spectra were calibrated, background corrected, and normalized, and a linear combination fitting procedure was used to obtain the relative abundance of Mn(II), Mn(III), and Mn(IV), as well as the Mn average oxidation state (Mn_{AOS},[46] Table S-1).

Soil Characterization. Total C and N content of each sample were determined on an elemental analyzer (Costech ECS 4010 CHNSO analyzer). Water extractable organic C (WEOC) was determined using a TOC analyzer (Shimadzu TOC-L/ASI-LAAS) on water extracts obtained in the sequential extraction procedure described above. Microbial biomass was determined by chloroform fumigation and subsequent extraction with K_2SO_4.[47] Total Mn and Fe contents were measured on composite samples (combining the four replicates) by X-ray fluorescence (Spectro Xepos HE XRF Spectometer).

Statistical Analysis. We performed all statistical analyses using R version 3.3.1. When necessary, we applied transformations to meet the assumptions of normality, evaluated with Shapiro-Wilk tests and Q-Q plots. We used linear mixed-effect models to identify the main effects of reactive Fe and Mn species, other biogeochemical parameters, position, and horizon on the rate of L-DOPA oxidation in our assays using the lme4 package.[48]

To identify variables to include in the model, we first explored pairwise linear relationships between oxidative activity and potential predictor variables. Oxidative activity with and without H_2O_2 additions showed the strongest correlations with pyrophosphate-, acetate-Mn, and total extractable Mn; HCl-extractable Fe(II) and total HCl-extractable Fe, total extractable Fe; as well as water extractable, microbial biomass, and total C (Table S-2 and Figure S-3). We then checked for covariance between these predictor variables. Because pyrophosphate-extractable Mn was strongly correlated with acetate- and total extractable Mn, HCl-extractable Fe with total extractable Fe, and microbial biomass C with water-extractable and total soil C ($R^2 > 0.5$), only the former set of variables was included in the model. Consequently, only pyrophosphate extractable Mn, HCl-extractable Fe(II), HCl-extractable Fe, and microbial biomass C were included in the model. This selection was deemed appropriate because it allowed us to contrast both Mn- and Fe-driven depolymerization pathways and offers the opportunity to assess the relative importance of microbial biomass as an indicator for predominantly enzymatically driven pathways.

Oxidative activity with and without H_2O_2 addition served as dependent variables in the model. Our model for the whole data set initially included pyrophosphate-extractable Mn, HCl-extractable Fe(II), total HCl-extractable Fe, and microbial biomass C, horizon (litter, organic, and mineral), and position (dry, transition, wet), as well as their interactive term (horizon x position), as fixed effects (independent variables). The random effect of the four transects sampled as well as the three landscape positions were used as a nested blocking factor to control for the random error associated with this sampling design. Similarly, we tested the effect of Fe and Mn phases, microbial biomass, and position in horizon-based models for each soil horizon. The horizon-based models included

https://dx.doi.org/10.1021/acs.est.0c04212
Environ. Sci. Technol. 2020, 54, 14114−14123

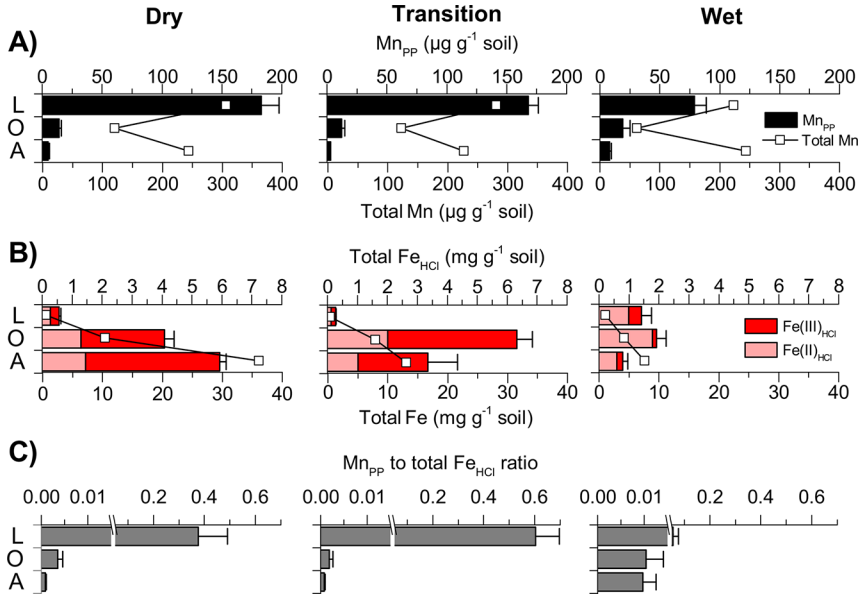

Figure 1. Concentrations of reactive Fe and Mn phases across the upland-to-wetland transect. (a) Pyrophosphate-extractable Mn (Mn_{PP}) and (b) total HCl-extractable Fe (total Fe_{HCl}), with proportions of Fe(II) and Fe(III) concentrations. Mn_{PP} and Total Fe_{HCl} concentrations (bar plots) are plotted on the top *x*-axis, while total Mn and Fe concentrations as determined by XRF (open square symbols) are shown for comparison on the bottom *x*-axis. (C) Ratio of pyrophosphate-extractable Mn (Mn_{PP}) and total HCl-extractable Fe (total Fe_{HCl}). L = litter layer, O = O-horizon, and A = mineral soil. Error bars denote standard error of the mean (n = 4).

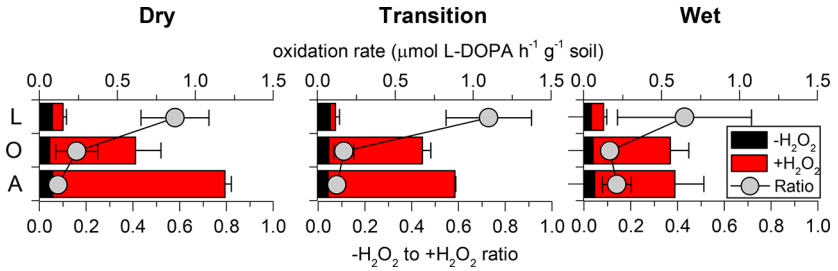

Figure 2. L-DOPA oxidation rates, a proxy for soil oxidative activity, across the upland-to-wetland transect. Oxidative activity is reported for assays conducted without ("baseline oxidative activity", black) and with H_2O_2 additions ("H_2O_2-dependent oxidative activity", red). The sum of both activities indicates total oxidative activity, while the ratio indicates the relative contribution of baseline (black) and H_2O_2-dependent (red) oxidative activity. L = litter layer, O = O-horizon, and A = mineral soil. Error bars denote standard error of the mean (n = 4).

pyrophosphate-extractable Mn, HCl-extractable Fe(II), HCl-extractable Fe, and microbial biomass C, and position as fixed effects, with transect as the blocking factor (random effect). The model residuals were not improved by log transformation of the dependent variable. We then eliminated insignificant independent variables (fixed effects) in a stepwise (reverse) fashion. In each step, the independent variables (fixed effects) with the highest p values, as assess by type III analysis of variance (ANOVA), were dropped from the model. The stepwise elimination of variables conduced in reverse (as described above) and forward fashion were consistent. Data for predictor variables were standardized to soil mass and allow direct comparisons by us to compare their relative strengths as predictor variables using the resulting F values and beta coefficients. No significant variables were identified in the model for the O horizons, possibly due to the more variable data set, which was thus not included in the results.

RESULTS

Soil Characteristics. Across our upland-to-wetland transect, total C, microbial biomass C (MB-C), and water-extractable C consistently decreases with depth but did not significantly differ among positions (Table 1). Total Mn concentrations consistently peaked in the litter layer, declined in the organic horizons, and increased in the mineral horizon, and total Fe concentrations increased with depth (Table 1). Consequently, total Mn-to-Fe ratios were more than 1 order of magnitude greater in the litter layer (0.2−0.6) than in organic (0.01−0.02) and mineral horizons (0.01−0.03).

Abundance of Reactive Mn and Fe Species Across the Upland-to-Wetland Transect. Concentrations of reactive Fe and Mn species varied with depth and redox gradients across our transect (Figure 1). Pyrophosphate-extractable (Mn_{PP}) was most abundant in the litter layer and decreases with depth. Conversely, both HCl-extractable Fe(II) ($Fe(II)_{HCl}$) and Fe(III) concentrations ($Fe(III)_{HCl}$) generally increased with depth, with the relative proportion of $Fe(II)_{HCl}$ increasing from dry to wet soils. The ratio of Mn_{PP} to total Fe_{HCl} (sum of Fe(II) and Fe(III)) generally declined with depth. While the average oxidation state of Fe covered the full spectrum 2.1−2.8, that of Mn was generally much lower 2.03−2.16 (Table S-1). Mn_{PP} accounted for more than 94% of the total extractable Mn in all samples (except for the A horizon in the dry position, where Mn_{PP} accounts for 54% of the total

https://dx.doi.org/10.1021/acs.est.0c04212
Environ. Sci. Technol. 2020, 54, 14114−14123

extractable pool), indicating that Mn present in our soils is predominantly organically bound (Figure S-1). Further, Mn_{PP} was well correlated with Mn(III) as determined by Mn K-edge XANES on composite samples (Figure S-2) and Mn(IV) was largely absent from our soils (Table S-1), suggesting that most of the oxidized and reactive Mn is present as organically complexed Mn(III), rather than crystalline Mn(III,IV) oxides. Together, these measurements demonstrate that organically complexed Mn, possibly dominated by reactive Mn(III), is most prevalent in the litter layer, while the abundance of reactive Fe phases increases in organic and mineral horizons.

Oxidative Activity Across Upland-to-Wetland Transect. L-DOPA assays allowed us to distinguish baseline oxidative activity (i.e., L-DOPA oxidation without H_2O_2 additions), H_2O_2-promoted oxidative activity (i.e., L-DOPA oxidation with H_2O_2 additions minus L-DOPA oxidation without H_2O_2 additions), and total oxidative activity (i.e., L-DOPA oxidation with H_2O_2 addition; Figure 2). Our results showed that oxidative activity without H_2O_2 additions ($-H_2O_2$) remained relatively constant with depth. L-DOPA assays receiving additions of H_2O_2 ($+H_2O_2$) showed increasing oxidative activity with depth, but declined from dry to wet positions. As expected, oxidative activity without H_2O_2 additions ($-H_2O_2$) were consistently lower than rates measured with H_2O_2 additions ($+H_2O_2$), with the exception of the litter layer at the dry and transition position where oxidative activity is greater in the absence of H_2O_2 additions. The ratio of oxidative activity without H_2O_2 additions ($-H_2O_2$) relative to the total oxidative activity is greatest in the litter layer and declines with depth. Combined, our results demonstrate that the baseline oxidative activity remains constant with depth but is proportionally strongest in the litter layer and that H_2O_2-promoted oxidative activity becomes relatively more important in organic and mineral soils.

Relative Effect of Reactive Fe and Mn on Oxidative Activity. To account for spatial autocorrelation with depth or across landscape positions, we used a nested mixed effects model to identify the main predictors of L-DOPA oxidation across the gradient (Figure 3). We first build a model for the whole data set, eliminating insignificant variables in a stepwise fashion (Figure 3a). The best fit-model describing oxidative activity without H_2O_2 additions included Mn_{PP} as the variable with the most significant predictive power. In contrast, the best-fit model explaining oxidative activity with H_2O_2 additions included Total Fe_{HCl}, and to a lesser degree MB-C, with the most significant predictive power. The best-fit model based on data sets for the litter layer alone included Mn_{PP} as the most significant predictor of oxidative activity without H_2O_2 additions, while total Fe_{HCl} was found to be the more significant predictor of oxidative activity when H_2O_2 was added (Figure 3b). In contrast, a model for the mineral soil (Figure 3c) showed that oxidative activity were best predicted by $Fe(II)_{HCl}$ without H_2O_2 addition, but total Fe_{HCl} became the dominant predictor variable when H_2O_2 was added. In sum, these modeling results demonstrate that (1) Mn_{PP} drives oxidative activity when no H_2O_2 is added, i.e., without any sample alteration, while Total Fe_{HCl} becomes more important with the addition of H_2O_2, and (2) that Mn-mediated oxidative activity is more important in the litter layer, while Fe is more important in the mineral soil.

Increased Oxidative Activity in Response to the Addition of Reactive Mn and Fe Species. To further assess the contribution of reactive Mn and Fe species to oxidative activity in the L-DOPA assays, we ran positive controls in which we amended soil assays with Mn(III), Mn(II), Fe(II), or Fe(III). L-DOPA oxidation generally increased with increasing concentrations of Mn and Fe species in assays without H_2O_2 additions (Figure 4a). Both Mn(III) and Fe(II) additions proportionally increased oxidative activity by comparable margins. Mn(III) oxidized L-DOPA more rapidly, while Fe(II) showed slower initial rates but more complete oxidation over time (Figure S-4). In comparison to Mn(III) and Fe(II), Mn(II) additions only had a small effect on oxidative activity (Figure 4c), most likely because Mn(III) had to be (enzymatically) formed first. Surprisingly, Fe(III) additions stimulated oxidative activity as much as Fe(II) (Figure 4a). H_2O_2 additions increased Fe-mediated oxidative activity at all initiate Fe(II) and Fe(III) concentrations by almost 1 order of magnitude (Figure 4b). H_2O_2 additions had the opposite effect on Mn-mediated oxidative reactivity, decreasing Mn(III)-mediated oxidative activity by 6 (at high initial Mn(III) concentrations) to 50% (at low initial Mn(III) concentrations) and Mn(II)-mediated activity by 58% (at high Mn(III) concentrations) (Figure 4c). Our positive controls thus established that the presence of both Mn(III), Fe(II) and

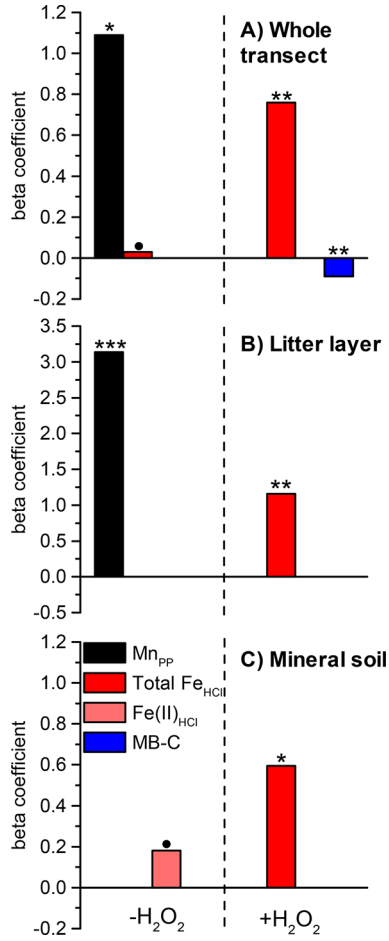

Figure 3. Coefficient strength of biogeochemical predictor variables for soil oxidative activity with and without H_2O_2 addition. Beta coefficients are reported for best-fits resulting nested linear mixed effects models for the (a) whole data set, (b) only the litter layer, and (c) only the mineral soil. Selected parameters included Mn_{PP}, total Fe_{HCl}, $Fe(II)_{HCl}$, and MB-C. Statistical significance is indicated at $p < 0.1$ (•), $p < 0.05$ (*), $p < 0.01$ (**), and $p < 0.001$ (***) levels. The complete fit parameters are given in Table S-3.

https://dx.doi.org/10.1021/acs.est.0c04212
Environ. Sci. Technol. 2020, 54, 14114−14123

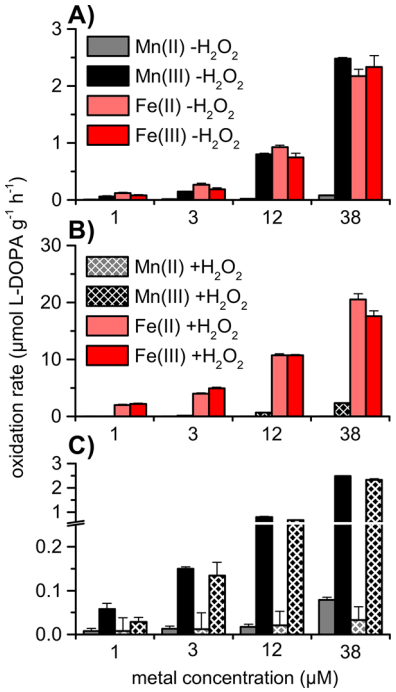

Figure 4. Oxidative activity in L-DOPA assays in response to the addition of reactive Mn and Fe species. Metal-induced oxidative activity (a) without H_2O_2 and (b) with H_2O_2 additions are shown. (c) Mn-mediated oxidative activity with and without H_2O_2 additions replotted to enable direct comparison. L-DOPA oxidation rates were calculated based on incubation times of 1 h. Error bars denote standard error of the mean (n = 3).

Fe(III) cause comparable levels of oxidative activity in soils. But the addition of H_2O_2 dramatically enhanced Fe-mediated and suppressed Mn-mediated oxidative activity.

DISCUSSION

Reactive Fe and Mn Species Best Predict Oxidative Activity. Recent evidence suggested that abiotic mechanisms drive oxidative decomposition in soils.[9−11,13] Our detailed examination of forest soil depth profiles shows that most of the oxidative activity can be explained by reactive Fe[13] and Mn phases,[28] rather than other measured soil properties. Oxidative activity was more strongly correlated to the abundance of reactive Fe and Mn phases than measures typically used to infer microbial and enzymatic activity (Figure 3A). Total, bioavailability, and microbial biomass C decreased with depth (Table 1), consistent with decreased microbial abundance[49] and enzymatic activity[50] in other forest soils. If oxidative activity was exclusively mediated via extracellular enzymes, we may thus expect that oxidative activity is greatest at the surface. However, in spite of seemingly declining microbial contributions, oxidative activity either remained constant (-H_2O_2) or increased with depth (+H_2O_2; Figure 2). Furthermore, even when assessed on an individual horizon basis using our mixed effects model, reactive Fe and Mn phases better predict oxidative activity than other measured parameters (Figure 3B and C). Finally, our positive controls confirmed the direct effect of both reactive Mn and Fe phases on oxidative activity (Figure 4). In sum, our results suggest that oxidative activity in forest soils is, in large parts, a reflection of oxidation reactions mediated by reactive Fe and Mn species.

Mn(III) Drives Oxidative Activity in Organic Layers and Fe(II) in Mineral Soils. Our results showed that variations in baseline oxidative activity (measured in assays without H_2O_2 additions most similar to baseline field conditions) across litter, organic, and mineral horizons were best explained by differences in the abundance of Mn(III) and Fe(II). In the litter layer, the greater contribution of baseline oxidative activity to total oxidative activity (Figure 2) coincided with the largest abundance of Mn(III) (Figure 1). Consequently, baseline oxidative activity in the litter layer was best predicted by Mn(III) in our mixed effects model (Figure 3B). Baseline oxidative activity remained relatively constant with depth and, while the abundance of Mn(III) significantly decreased with depth, that of Fe(II) increased (Figure 1). Accordingly, our mixed model identified Fe(II) as the strongest predictor of baseline oxidative activity in mineral soils (Figure 3C). Our results thus confirm our initial assumption that oxidative decomposition in the litter layer is principally driven by Mn(III)-mediated reactions,[28] while Fe(II)-mediated strategies are relatively more important in the mineral soil.[13]

The comparison of assays conducted with and without H_2O_2 additions provides further insights into the relative contribution of Mn- and Fe-mediated oxidative decomposition. Without H_2O_2 additions, meaning under assay conditions most similar to baseline field conditions, Mn(III) best explained oxidative activity in our model for the whole transect (Figure 3A). Conversely, when H_2O_2 was added to assays, Fe became by far the better predictor of oxidative activity at our field site (Figure 3A). Our control experiments further showed that H_2O_2 additions dramatically enhanced not just Fe(II), but also Fe(III)-mediated L-DOPA oxidation rates, while holding constant or suppressing Mn(III) and Mn(II)-mediated L-DOPA oxidation rates (Figure 4B). This observation is in agreement with the well-known stimulation of Fenton chemical reactions by H_2O_2,[34] either produced biotically or abiotically,[27] as well as the H_2O_2-mediated inhibition of Mn(II) oxidation and reduction of reactive Mn(III) species.[33] Baseline oxidative activity in unamended assays thus appeared to be more sensitive to Mn(III)-mediated oxidative decomposition,[28] while assays receiving H_2O_2 additions capture Fe-mediated oxidative decomposition.[13]

These findings have important implications for the interpretation of oxidative activity measurements in organic and mineral soils globally.[51] Across a range of forest and grassland ecosystems, the ratio of oxidative activity without H_2O_2 and oxidative activity with H_2O_2 is almost an order of magnitude greater in the litter layer (2.4 ± 1.3) than in the mineral soil (0.3 ± 0.1).[52−54] In other words, the relative contribution of baseline oxidative activity is consistently greater in the litter layer, while that of H_2O_2-promoted activity tends to be greater in the mineral soil. If we now assume, as supported by our results, that oxidative activity in assays without H_2O_2 is more sensitive to Mn(III) whereas oxidative activity in assays receiving H_2O_2 is primarily driven by Fe, these broad trends suggest that Mn(III)-driven mechanisms[40] may explain oxidative activity in organic layers, while Fe-driven mechanisms[13] may be responsible for measured oxidative activities in minerals soils across a variety of ecosystems.

The proposed differentiation of Mn- versus Fe-mediated oxidative mechanisms with depth are consistent with a recent study of fungal abundances and oxidative activity across organic and mineral forest soils at the continental scale.[51,55]

https://dx.doi.org/10.1021/acs.est.0c04212
Environ. Sci. Technol. 2020, 54, 14114−14123

That study found saprotrophic basidiomycetes to dominate organic layers, which are generally enriched in Mn.[30] Conversely, fungal communities tend to be dominated by mycorrhizal fungi in minerals soils,[51] which are relatively more enriched in Fe.[30] Interestingly, saprotrophic white rot fungi also generated by far the highest baseline oxidative activity (i.e., without H_2O_2 additions) compared to other fungal groups.[51] In contrast, ectomycorrhizal fungi produced significant H_2O_2-dependent oxidative activity, possibly due to their reliance on nonenzymatic, Fe-driven mechanisms.[25] Our results therefore suggest a depth-differentiation of oxidative pathways, in which fungal decomposer organisms adapted specific metal-mediated strategies depending on the relative abundance and availability of Mn and Fe in organic and mineral soils.

Implications for Assessing Oxidative Activity in Soils. Our results provide important insights into the utility of L-DOPA to assess the quantitative roles of reactive Fe and Mn species in mediating oxidative activity in soils. While both Mn(III) and Fe(II/III) readily oxidize L-DOPA (Figure 4a) and, combined, predicted most of the oxidative activity across our soils (Figure 3), they behaved differently in ways that affect how we can assess their relative contribution in L-DOPA assays and how such oxidative activity assays should be interpreted more generally.

First, incubations times influence the sensitivity of L-DOPA assays to Mn- and Fe-mediated oxidation and, thus, their relative contributions to oxidative activity measurements. Our positive controls amended with either Mn or Fe species, Mn-mediated L-DOPA oxidation peaked within the first hour. By comparison, Fe-mediated oxidation was relatively constant throughout the assay duration (Figure S-4). L-DOPA assays to measure oxidative activity are generally conducted across a wide range of incubation times: from 5[56] and 60 min[13] to 4,[31] 5,[32] 24,[52,53] or even 48 h.[38] At an incubation time of 4 h, used to assess oxidative activity in this study, Mn- and Fe-mediated L-DOPA oxidation proceeded at comparable rates (Figure S-4). We thus do not expect any systemic bias toward either Mn- or Fe-mediated oxidative activity measurements across our upland-to-wetland transect (Figure 2). However, these results suggest studies of soil oxidative activities relying on shorter incubation times[13,56] are more likely to capture Mn-mediated oxidative activity, while longer incubation times[38,52,53] measure a greater contribution of Fe-mediated oxidative activity.

Second, autocatalytic reactions between L-DOPA and Fe appear to perpetuate Fe-driven L-DOPA oxidation in the assay. In our positive controls, Fe(III)-mediated L-DOPA oxidation was almost identical to that of Fe(II) (Figure 4), and remained constant over time (Figure S-4). The surprisingly high oxidative activity in response to Fe(III) additions suggests that Fe(III) is rapidly reduced to Fe(II), which then prompts Fenton-mediated oxidation of L-DOPA. It is plausible that the L-DOPA, a phenolic compound with structural similarities to strong reductants such as catechol[57,58] and other dihydrophenols,[59,60] reacts with Fe(III) to continuously regenerate Fe(II). L-DOPA oxidation, in turn, then produces a quinone, L-dopaquinone, which have been shown to catalyze Fe(II) oxidation.[60] Such autocatalytic reactions between the Fe(II)/(III) redox couple and the phenol/quinone redox mediator, if oxygen is present,[13] can results in continuous regeneration of reactive oxygen species.[59,60] This process would explain the relatively constant, seemingly self-perpetuating Fe-mediated L-DOPA oxidation throughout our assay incubations (Figure S-4). Such autocatalytic behavior was not observed for Mn-mediated L-DOPA oxidation. Instead, Mn(III)-mediated oxidation dropped sharply after the first hour (Figure S-4), most likely because all of the Mn(III) had reacted. The fact that Mn(II) amended assays showed extremely low L-DOPA oxidation suggests that very little reactive Mn(III) is generated in the assays. Moreover, as mentioned above, while the addition of H_2O_2 as an oxidant dramatically enhanced Fe-mediated L-DOPA oxidation, it suppressed Mn-mediated L-DOPA oxidation (Figure 4B). Combined, these results show that the excess amount of a redox mediator[60] (i.e., L-DOPA/L-dopaquinone) and oxidant[13] (O_2 or H_2O_2), continuously perpetuate Fe-driven L-DOPA oxidation in the assays, but have no or even inhibitive effects on Mn-mediated L-DOPA oxidation. Under natural soil conditions, the supply of natural redox mediators and H_2O_2 production driving Fe-mediated L-DOPA oxidation is expected to be finite. Our findings therefore suggest that conventional assays of oxidative activity overestimate the quantitative role of Fe and, in turn, underestimate the potential contribution of reactive Mn species.

Importance of Coupled Abiotic−Biotic Processes in Oxidative Decomposition in Soils. Our investigation shows that oxidative activity in soils is, in large parts, linked to the abundance of reactive Mn and Fe species. Oxidative decomposition is therefore not only a reflection of enzymatic activity, but also the cycling of reactive Mn(III)[28,41] and Fe(II)[13,16] intermediates. Our results demonstrate that Mn-(III)-mediated pathways drive oxidative activity in Mn-enriched surface litter, while Fe(II)-mediated reactions dominate Fe-richer mineral soils. These findings suggest that microbes utilize different metal-mediated, oxidative depolymerization pathways depending on the relative availability of Mn and Fe in a given soil environment. Efforts to accurately model oxidative activity in microbially explicit models[6,7] will thus necessitate explicit consideration of the distribution, reactivity, and cycling of metal intermediates to predict how future environmental change may affect microbial OM decomposition rates.

While our findings agree with recent assertions that a significant amount of oxidative activity in soils is generated through abiotic reactions,[9−11] it is important to note that Fe- and Mn-mediated oxidative decomposition cannot be regarded as exclusively abiotic processes. Fe(II)-mediated organic matter decomposition necessitates Fe(III) reduction to produce reactive Fe(II),[13,27] which is most frequently mediated by bacteria[61] or fungi[18,24] through reductive enzymes or metabolites. Similarly, Mn(II) oxidation to create reactive Mn(III) is also thought to be predominantly microbially mediated.[28,41,62] It has been shown that reactive intermediates, such as Fe(II), persist even through sterilization treatments,[13] which are used to assess abiotic contributions in the aforementioned studies.[9−11] Consequently, while reactive Fe and Mn appear to be the principal drivers of oxidative activity, our results are indicative of a tight redox coupling between biotic, enzymatically-driven and abiotic, metal-mediated reactions in organic matter decomposition. Future studies using molecular approaches may shed additional light on the tight interplay between microbes, their oxidative enzymes, and metal cycling that facilitates oxidative decomposition in soils.

https://dx.doi.org/10.1021/acs.est.0c04212
Environ. Sci. Technol. 2020, 54, 14114−14123

■ ASSOCIATED CONTENT

Supporting Information

The Supporting Information is available free of charge at https://pubs.acs.org/doi/10.1021/acs.est.0c04212.

Mn XANES fitting results; pairwise linear regression results; nested linear mixed effects model parameters; extractable Fe and Mn pools; L-DOPA oxidation in response to Fe and Mn additions (PDF)

■ AUTHOR INFORMATION

Corresponding Author

Marco Keiluweit − *School of Earth & Sustainability and Stockbridge School of Agriculture, University of Massachusetts, Amherst, Massachusetts 01003, United States;* orcid.org/0000-0002-7061-8346; Email: Keiluweit@umass.edu

Authors

Morris E. Jones − *School of Earth & Sustainability and Stockbridge School of Agriculture, University of Massachusetts, Amherst, Massachusetts 01003, United States; Department of Chemistry, Franklin Pierce University, Rindge, New Hampshire 03461, United States*

Rachelle E. LaCroix − *School of Earth & Sustainability and Stockbridge School of Agriculture, University of Massachusetts, Amherst, Massachusetts 01003, United States*

Jacob Zeigler − *School of Earth & Sustainability and Stockbridge School of Agriculture, University of Massachusetts, Amherst, Massachusetts 01003, United States*

Samantha C. Ying − *Department of Environmental Science, University of California—Riverside, Riverside, California 92521, United States;* orcid.org/0000-0002-1247-2529

Peter S. Nico − *Environmental and Earth Science Division, Lawrence Berkeley National Laboratory, Berkeley, California 94720, United States*

Complete contact information is available at: https://pubs.acs.org/10.1021/acs.est.0c04212

Notes

The authors declare no competing financial interest.

■ ACKNOWLEDGMENTS

The authors thank B. Goodell and N. A. Chin (UMass Amherst) for fruitful discussions, Harvard Forest REU students A. Skora-Rivera, S. Pardi, and M. Wilcots for assistance with sample collection and analysis, and Steven Hall and Xiaojuan Feng as well as two additional anonymous reviewers for their constructive comments and suggestions. The authors also acknowledge support from the Harvard Forest REU and LTER programs (Award No. NSF-DEB 1237491). Use of SSRL at the Stanford Linear Accelerator Center National Accelerator Laboratory is supported by the U.S. Department of Energy, Office of Science, Office of Basic Energy Sciences under contract DE-AC02-76SF00515. This work was funded by the NSF Geobiology & Low-temperature Geochemistry program (Award No. 1852754 to M.K.).

■ REFERENCES

(1) Köchy, M.; Hiederer, R.; Freibauer, A. Global Distribution of Soil Organic Carbon − Part 1: Masses and Frequency Distributions of SOC Stocks for the Tropics, Permafrost Regions, Wetlands, and the World*SOIL*, **2015**1351365.

(2) Bradford, M. A.; Berg, B.; Maynard, D. S.; Wieder, W. R.; Wood, S. A. Understanding the Dominant Controls on Litter Decomposition. *J. Ecol.* **2016**, *104* (1), 229−238.

(3) Heimann, M.; Reichstein, M. Terrestrial Ecosystem Carbon Dynamics and Climate Feedbacks. *Nature* **2008**, *451* (7176), 289−292.

(4) Meentemeyer, V. Macroclimate the Lignin Control of Litter Decomposition Rates. *Ecology* **1978**, *59* (3), 465−472.

(5) Sinsabaugh, R. L. Phenol Oxidase, Peroxidase and Organic Matter Dynamics of Soil. *Soil Biol. Biochem.* **2010**, *42* (3), 391−404.

(6) Allison, S. D.; Wallenstein, M. D.; Bradford, M. A. Soil-Carbon Response to Warming Dependent on Microbial Physiology. *Nat. Geosci.* **2010**, *3* (5), 336−340.

(7) Wieder, W. R.; Bonan, G. B.; Allison, S. D. Global Soil Carbon Projections Are Improved by Modelling Microbial Processes. *Nat. Clim. Change* **2013**, *3* (10), 909−912.

(8) Wang, B.; Allison, S. D. Emergent Properties of Organic Matter Decomposition by Soil Enzymes. *Soil Biol. Biochem.* **2019**, *136*, 107522.

(9) Blankinship, J. C.; Becerra, C. A.; Schaeffer, S. M.; Schimel, J. P. Separating Cellular Metabolism from Exoenzyme Activity in Soil Organic Matter Decomposition. *Soil Biol. Biochem.* **2014**, *71*, 68−75.

(10) Kéraval, B.; Lehours, A. C.; Colombet, J.; Amblard, C.; Alvarez, G.; Fontaine, S. Soil Carbon Dioxide Emissions Controlled by an Extracellular Oxidative Metabolism Identifiable by Its Isotope Signature. *Biogeosciences* **2016**, *13* (22), 6353−6362.

(11) Kéraval, B.; Fontaine, S.; Lallement, A.; Revaillot, S.; Billard, H.; Alvarez, G.; Maestre, F.; Amblard, C.; Lehours, A.-C. Cellular and Non-Cellular Mineralization of Organic Carbon in Soils with Contrasted Physicochemical Properties. *Soil Biol. Biochem.* **2018**, *125*, 286−289.

(12) Sun, T.; Cui, Y.; Berg, B.; Zhang, Q.; Dong, L.; Wu, Z.; Zhang, L. A Test of Manganese Effects on Decomposition in Forest and Cropland Sites. *Soil Biol. Biochem.* **2019**, *129*, 178−183.

(13) Hall, S. J.; Silver, W. L. Iron Oxidation Stimulates Organic Matter Decomposition in Humid Tropical Forest Soils. *Glob Change Biol.* **2013**, *19* (9), 2804−2813.

(14) Kranabetter, J. M. Increasing Soil Carbon Content with Declining Soil Manganese in Temperate Rainforests: Is There a Link to Fungal Mn? *Soil Biol. Biochem.* **2019**, *128*, 179−181.

(15) Trusiak, A.; Treibergs, L. A.; Kling, G. W.; Cory, R. M. The Role of Iron and Reactive Oxygen Species in the Production of CO2 in Arctic Soil Waters. *Geochim. Cosmochim. Acta* **2018**, *224*, 80−95.

(16) Wang, Y.; Wang, H.; He, J.-S.; Feng, X. Iron-Mediated Soil Carbon Response to Water-Table Decline in an Alpine Wetland. *Nat. Commun.* **2017**, *8*, 15972.

(17) Van Bodegom, P. M.; Broekman, R.; Van Dijk, J.; Bakker, C.; Aerts, R. Ferrous Iron Stimulates Phenol Oxidase Activity and Organic Matter Decomposition in Waterlogged Wetlands. *Biogeochemistry* **2005**, *76* (1), 69−83.

(18) Cragg, S. M.; Beckham, G. T.; Bruce, N. C.; Bugg, T. D.; Distel, D. L.; Dupree, P.; Etxabe, A. G.; Goodell, B. S.; Jellison, J.; McGeehan, J. E.; McQueen-Mason, S. J.; Schnorr, K.; Walton, P. H.; Watts, J. E.; Zimmer, M. Lignocellulose Degradation Mechanisms across the Tree of Life. *Curr. Opin. Chem. Biol.* **2015**, *29*, 108−119.

(19) Hofrichter, M. Review: Lignin Conversion by Manganese Peroxidase (MnP). *Enzyme Microb. Technol.* **2002**, *30* (4), 454−466.

(20) Perez, J.; Jeffries, T. W. Roles of Manganese and Organic Acid Chelators in Regulating Lignin Degradation and Biosynthesis of Peroxidases by Phanerochaete Chrysosporium. *Appl. Environ. Microbiol.* **1992**, *58* (8), 2402−2409.

(21) Hansel, C. M. Manganese in Marine Microbiology. In *Advances in Microbial Physiology*; Elsevier: Amsterdam, 2017; Vol. *70*, pp 37−83.

(22) Shah, F.; Nicolás, C.; Bentzer, J.; Ellström, M.; Smits, M.; Rineau, F.; Canbäck, B.; Floudas, D.; Carleer, R.; Lackner, G.; Braesel, J.; Hoffmeister, D.; Henrissat, B.; Ahrén, D.; Johansson, T.; Hibbett, D. S.; Martin, F.; Persson, P.; Tunlid, A. Ectomycorrhizal Fungi Decompose Soil Organic Matter Using Oxidative Mechanisms

Adapted from Saprotrophic Ancestors. *New Phytol.* **2016**, *209* (4), 1705−1719.
(23) Rineau, F.; Roth, D.; Shah, F.; Smits, M.; Johansson, T.; Canbäck, B.; Olsen, P. B.; Persson, P.; Grell, M. N.; Lindquist, E.; Grigoriev, I. V.; Lange, L.; Tunlid, A. The Ectomycorrhizal Fungus Paxillus Involutus Converts Organic Matter in Plant Litter Using a Trimmed Brown-Rot Mechanism Involving Fenton Chemistry. *Environ. Microbiol.* **2012**, *14* (6), 1477−1487.
(24) Shah, F.; Schwenk, D.; Nicolás, C.; Persson, P.; Hoffmeister, D.; Tunlid, A. Involutin Is an Fe3+ Reductant Secreted by the Ectomycorrhizal Fungus Paxillus Involutus during Fenton-Based Decomposition of Organic Matter. *Appl. Environ. Microbiol.* **2015**, *81* (24), 8427−8433.
(25) Op De Beeck, M.; Troein, C.; Siregar, S.; Gentile, L.; Abbondanza, G.; Peterson, C.; Persson, P.; Tunlid, A. Regulation of Fungal Decomposition at Single-Cell Level. *ISME J.* **2020**, *14* (4), 896−905.
(26) Trusiak, A.; Treibergs, L. A.; Kling, G. W.; Cory, R. M. The Controls of Iron and Oxygen on Hydroxyl Radical (•OH) Production in Soils. *Soil Systems* **2019**, *3* (1), 1.
(27) Pignatello, J. J.; Oliveros, E.; MacKay, A. Advanced Oxidation Processes for Organic Contaminant Destruction Based on the Fenton Reaction and Related Chemistry. *Crit. Rev. Environ. Sci. Technol.* **2006**, *36* (1), 1−84.
(28) Keiluweit, M.; Nico, P.; Harmon, M. E.; Mao, J.; Pett-Ridge, J.; Kleber, M. Long-Term Litter Decomposition Controlled by Manganese Redox Cycling. *Proc. Natl. Acad. Sci. U. S. A.* **2015**, *112* (38), E5253−E5260.
(29) Herndon, E. M.; Martínez, C. E.; Brantley, S. L. Spectroscopic (XANES/XRF) Characterization of Contaminant Manganese Cycling in a Temperate Watershed. *Biogeochemistry* **2014**, *121* (3), 505−517.
(30) Kaste, J. M.; Bostick, B. C.; Heimsath, A. M.; Steinnes, E.; Friedland, A. J. Using Atmospheric Fallout to Date Organic Horizon Layers and Quantify Metal Dynamics during Decomposition. *Geochim. Cosmochim. Acta* **2011**, *75* (6), 1642−1661.
(31) Bach, C. E.; Warnock, D. D.; Van Horn, D. J.; Weintraub, M. N.; Sinsabaugh, R. L.; Allison, S. D.; German, D. P. Measuring Phenol Oxidase and Peroxidase Activities with Pyrogallol, l-DOPA, and ABTS: Effect of Assay Conditions and Soil Type. *Soil Biol. Biochem.* **2013**, *67*, 183−191.
(32) DeForest, J. L. The Influence of Time, Storage Temperature, and Substrate Age on Potential Soil Enzyme Activity in Acidic Forest Soils Using MUB-Linked Substrates and l-DOPA. *Soil Biol. Biochem.* **2009**, *41* (6), 1180−1186.
(33) Learman, D. R.; Voelker, B. M.; Madden, A. S.; Hansel, C. M. Constraints on Superoxide Mediated Formation of Manganese Oxides. *Front. Microbiol.* **2013**, *4*, 4.
(34) Bissey, L. L.; Smith, J. L.; Watts, R. J. Soil Organic Matter-Hydrogen Peroxide Dynamics in the Treatment of Contaminated Soils and Groundwater Using Catalyzed H2O2 Propagations (Modified Fenton's Reagent). *Water Res.* **2006**, *40* (13), 2477−2484.
(35) Phillips, S. C.; Varner, R. K.; Frolking, S.; Munger, J. W.; Bubier, J. L.; Wofsy, S. C.; Crill, P. M. Interannual, Seasonal, and Diel Variation in Soil Respiration Relative to Ecosystem Respiration at a Wetland to Upland Slope at Harvard Forest. *J. Geophys. Res.* **2010**, *115* (G2), G02019.
(36) Brooks, R. T. A Review of Basin Morphology and Pool Hydrology of Isolated Ponded Wetlands: Implications for Seasonal Forest Pools of the Northeastern United States. *Wetlands Ecol. Manage.* **2005**, *13* (3), 335−348.
(37) LaCroix, R. E.; Tfaily, M. M.; McCreight, M.; Jones, M. E.; Spokas, L.; Keiluweit, M. Shifting Mineral and Redox Controls on Carbon Cycling in Seasonally Flooded Mineral Soils. *Biogeosciences* **2019**, *16* (13), 2573−2589.
(38) Pold, G.; Melillo, J. M.; DeAngelis, K. M. Two Decades of Warming Increases Diversity of a Potentially Lignolytic Bacterial Community. *Front. Microbiol.* **2015**, *6*, 6.
(39) Kostka, J. E.; Luther, G. W.; Nealson, K. H. Chemical and Biological Reduction of Mn (III)-Pyrophosphate Complexes: Potential Importance of Dissolved Mn (III) as an Environmental Oxidant. *Geochim. Cosmochim. Acta* **1995**, *59* (5), 885−894.
(40) Keiluweit, M.; Bougoure, J. J.; Nico, P. S.; Pett-Ridge, J.; Weber, P. K.; Kleber, M. Mineral Protection of Soil Carbon Counteracted by Root Exudates. *Nat. Clim. Change* **2015**, *5* (6), 588−595.
(41) Jones, M. E.; Nico, P. S.; Ying, S.; Regier, T.; Thieme, J.; Keiluweit, M. Manganese-Driven Carbon Oxidation at Oxic-Anoxic Interfaces. *Environ. Sci. Technol.* **2018**, *52* (21), 12349−12357.
(42) Nico, P. S.; Zasoski, R. J. Mn(III) Center Availability as a Rate Controlling Factor in the Oxidation of Phenol and Sulfide on δ-MnO$_2$. *Environ. Sci. Technol.* **2001**, *35* (16), 3338−3343.
(43) Stookey, L. L. Ferrozine—a New Spectrophotometric Reagent for Iron. *Anal. Chem.* **1970**, *42* (7), 779−781.
(44) Guest, C. A.; Schulze, D. G.; Thompson, I. A.; Huber, D. M. Correlating Manganese X-Ray Absorption near-Edge Structure Spectra with Extractable Soil Manganese. *Soil Science Society of America Journal* **2002**, *66* (4), 1172−1181.
(45) Chao, T. T. Selective Dissolution of Manganese Oxides from Soils and Sediments with Acidified Hydroxylamine Hydrochloride 1. *Soil Science Society of America Journal* **1972**, *36* (5), 764−768.
(46) Manceau, A.; Marcus, M. A.; Grangeon, S. Determination of Mn Valence States in Mixed-Valent Manganates by XANES Spectroscopy. *Am. Mineral.* **2012**, *97* (5−6), 816−827.
(47) Vance, E. D.; Brookes, P. C.; Jenkinson, D. S. An Extraction Method for Measuring Soil Microbial Biomass C. *Soil Biol. Biochem.* **1987**, *19* (6), 703−707.
(48) Bates, D.; Mächler, M.; Bolker, B.; Walker, S. Fitting Linear Mixed-Effects Models Using Lme4. *Journal of Statistical Software* **2015**, *67* (1), 1−48.
(49) Agnelli, A.; Ascher, J.; Corti, G.; Ceccherini, M. T.; Nannipieri, P.; Pietramellara, G. Distribution of Microbial Communities in a Forest Soil Profile Investigated by Microbial Biomass, Soil Respiration and DGGE of Total and Extracellular DNA. *Soil Biol. Biochem.* **2004**, *36* (5), 859−868.
(50) Stone, M. M.; DeForest, J. L.; Plante, A. F. Changes in Extracellular Enzyme Activity and Microbial Community Structure with Soil Depth at the Luquillo Critical Zone Observatory. *Soil Biol. Biochem.* **2014**, *75*, 237−247.
(51) Talbot, J. M.; Martin, F.; Kohler, A.; Henrissat, B.; Peay, K. G. Functional Guild Classification Predicts the Enzymatic Role of Fungi in Litter and Soil Biogeochemistry. *Soil Biol. Biochem.* **2015**, *88*, 441−456.
(52) Gallo, M.; Amonette, R.; Lauber, C.; Sinsabaugh, R. L.; Zak, D. R. Microbial Community Structure and Oxidative Enzyme Activity in Nitrogen-Amended North Temperate Forest Soils. *Microb. Ecol.* **2004**, *48* (2), 218−229.
(53) Sinsabaugh, R. L.; Gallo, M. E.; Lauber, C.; Waldrop, M. P.; Zak, D. R. Extracellular Enzyme Activities and Soil Organic Matter Dynamics for Northern Hardwood Forests Receiving Simulated Nitrogen Deposition. *Biogeochemistry* **2005**, *75* (2), 201−215.
(54) DeForest, J. L.; Zak, D. R.; Pregitzer, K. S.; Burton, A. J. Atmospheric Nitrate Deposition, Microbial Community Composition, and Enzyme Activity in Northern Hardwood Forests. *Soil Sci. Soc. Am. J.* **2004**, *68* (1), 132−138.
(55) Talbot, J. M.; Bruns, T. D.; Taylor, J. W.; Smith, D. P.; Branco, S.; Glassman, S. I.; Erlandson, S.; Vilgalys, R.; Liao, H.-L.; Smith, M. E.; Peay, K. G. Endemism and Functional Convergence across the North American Soil Mycobiome. *Proc. Natl. Acad. Sci. U. S. A.* **2014**, *111* (17), 6341−6346.
(56) Freeman, C.; Ostle, N.; Kang, H. An Enzymic "latch" on a Global Carbon Store. *Nature* **2001**, *409* (6817), 149−149.
(57) Santana-Casiano, J. M.; González-Dávila, M.; González, A. G.; Millero, F. J. Fe(III) Reduction in the Presence of Catechol in Seawater. *Aquat. Geochem.* **2010**, *16* (3), 467−482.
(58) Pracht, J.; Boenigk, J.; Isenbeck-Schröter, M.; Keppler, F.; Schöler, H. F. Abiotic Fe(III) Induced Mineralization of Phenolic Substances. *Chemosphere* **2001**, *44* (4), 613−619.

https://dx.doi.org/10.1021/acs.est.0c04212
Environ. Sci. Technol. 2020, 54, 14114−14123

(59) Salgado, P.; Melin, V.; Durán, Y.; Mansilla, H.; Contreras, D. The Reactivity and Reaction Pathway of Fenton Reactions Driven by Substituted 1,2-Dihydroxybenzenes. *Environ. Sci. Technol.* **2017**, *51* (7), 3687−3693.
(60) Yuan, X.; Davis, J. A.; Nico, P. S. Iron-Mediated Oxidation of Methoxyhydroquinone under Dark Conditions: Kinetic and Mechanistic Insights. *Environ. Sci. Technol.* **2016**, *50* (4), 1731−1740.
(61) Lovley, D. R. Dissimilatory Metal Reduction. *Annu. Rev. Microbiol.* **1993**, *47* (1), 263−290.
(62) Madison, A. S.; Tebo, B. M.; Mucci, A.; Sundby, B.; Luther, G. W. Abundant Porewater Mn(III) Is a Major Component of the Sedimentary Redox System. *Science* **2013**, *341* (6148), 875−878.

https://dx.doi.org/10.1021/acs.est.0c04212
Environ. Sci. Technol. 2020, 54, 14114−14123